# Study of the pore systems of solid catalysts by <sup>129</sup>Xe NMR

**Spectroscopic background:** <sup>129</sup>Xe nuclei have a spin of I = 1/2 and, therefore, no quadrupole moment. The <sup>129</sup>Xe isotope has a natural abundance of 26.4 %, a resonance frequency of  $v_0 = 139.09$  MHz at  $B_0 = 11.75$ , and a sensitivity of 5.7 x  $10^{-3}$  in comparison with <sup>1</sup>H nuclei (1.0). These properties make the <sup>129</sup>Xe isotope a suitable candidate for NMR studies of porous solids. For basic principles of solid-state NMR, see lectures "Solid-State NMR Spectroscopy" for Bachelor students or PhD seminars, accessible via the link "Lectures for Students".

NMR studies of adsorbed <sup>129</sup>Xe atoms provide a useful approach for **characterizing the pore systems of solid adsorbents and catalysts**. Assuming a fast exchange of xenon atoms adsorbed in the pores and cavities of porous solids, the observed <sup>129</sup>Xe chemical shift is described by the sum of several additive terms [1, 2]:

$$\delta_{129Xe} = \delta_0 + \delta_S + \delta_E + \delta_M + \delta_{Xe-Xe} \cdot \rho_{Xe}$$
 (1)

In a number of  $^{129}$ Xe NMR investigations performed at room temperature, the empirical **Eq. (1)** was utilized to characterize the void space and guest compounds in zeolite pores and cages. In Ref. [3], a model which allows the correlation of the  $\delta_{\rm S}$  term in **Eq. (1)** with the mean free path of a single  $^{129}$ Xe atom within the pores and cages. According to Ref. [4], the term  $\delta_{\rm S}$  depends on the fractional time, which the  $^{129}$ Xe atoms spend on the pore of cage walls. The effect of the surface curvature of zeolite pores or cages and of the adsorption energy on the term  $\delta_{\rm S}$  was discussed in Ref. [5]. Hence, there are several approaches leading to an estimation of the dimensions of the void spaces in porous solids by  $^{129}$ Xe NMR spectroscopy. For a review on the basic principles of  $^{129}$ Xe NMR spectroscopy, see Ref. [1].

In zeolites X and Y with  $n_{Si}/n_{Al}$  ratios of 1.2 to 50 and exchanged with univalent cations (Na+ and Li+) or H+, the interdependence of the  $^{129}$ Xe chemical shift and the xenon coverage is approximately linear [6]. This is due to the term  $\delta_{Xe-Xe} \cdot \rho_{Xe}$  in **Eq.** (1) arising from the two-body xenon-xenon collisions and indicates that for these zeolites the terms  $\delta_E$  and  $\delta_M$  can be neglected. Furthermore, the experimentally derived chemical shifts of  $^{129}$ Xe atoms are independent of the framework composition. In **Fig. 1**, the  $^{129}$ Xe chemical shifts,  $\delta_{129Xe}$ , of  $^{129}$ Xe atoms adsorbed on zeolites with different structure types are shown. All curves show an increase of the  $\delta_{129Xe}$  values with increasing xenon coverage, [Xe], which is, at least for low coverages, approximately linear. Extrapolation of the data to **[Xe] = 0 enables the determination of**  $\delta_S$ , which covers a range of ca. 60 ppm for zeolite Y and 113 ppm

# room-temperature <sup>129</sup>Xe chemical shifts for different zeolites

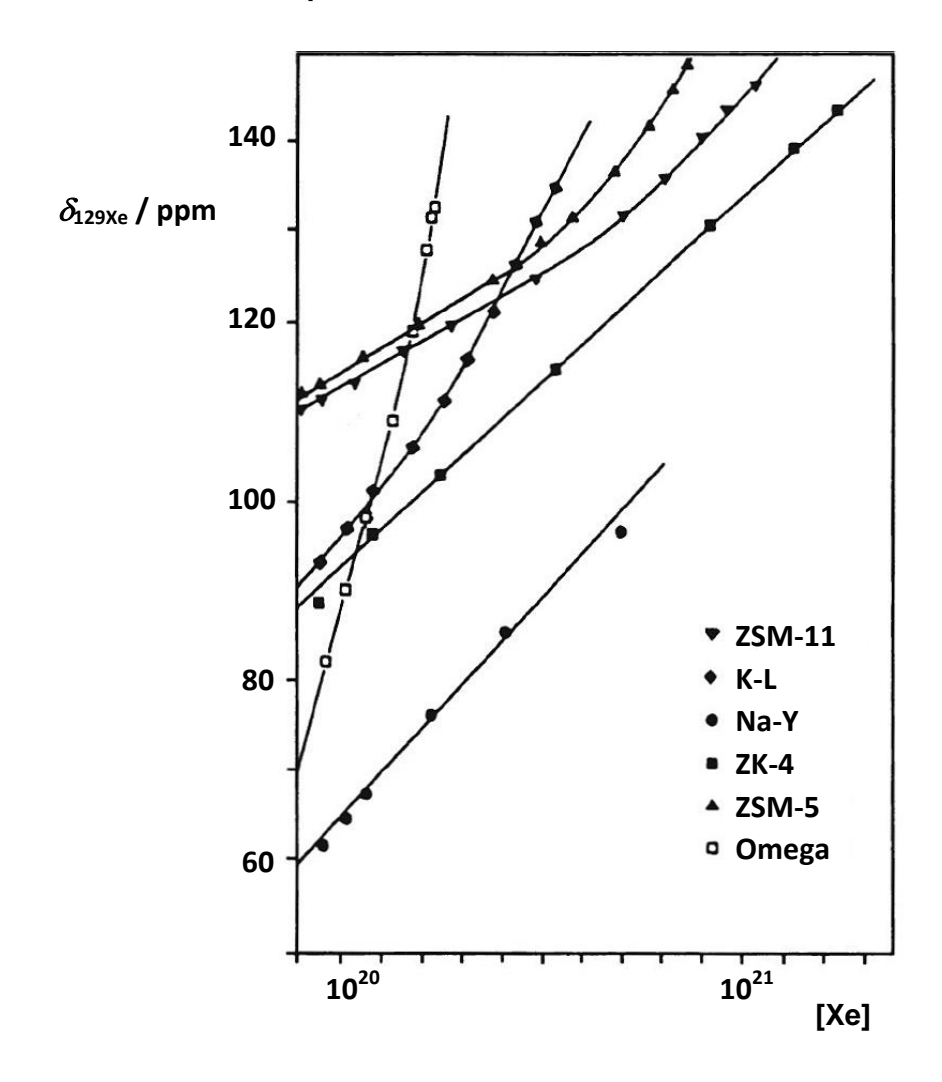


Fig. 1

for zeolite ZSM-5. The data given in **Table 1** demonstrate the relationship between  $\delta_{\rm S}$  and the pore size [1]. Terms  $\delta_{\rm S}$  derived for xenon atoms adsorbed on aluminophosphates and silicoaluminophosphates are given in Refs. [2] and [7-9]. For an introduction into the effect of multivalent cations, paramagnetic sites, and metal atoms in zeolites on the <sup>129</sup>Xe chemical shifts of adsorbed <sup>129</sup>Xe atoms, see the review in Ref. [1].

Zeolites	$\delta_{\! S}$ / ppm [1]	Cages and Pore Sizes [1]
X and Y	60	spherical supercages with $\emptyset \approx 1.3 \text{ nm}$
omega	73	unidimensional 12-ring pores with openings of 0.74 nm
A and ZK-4	87	spherical cages with $\varnothing \approx 1.14$ nm, six 8-ring openings with $\varnothing \approx 0.4$ – 0.5 nm
L	90	unidimensional 12-ring pores with openings of $\emptyset \approx 0.71$ nm, maximum $\emptyset \approx 0.9$ nm
ZSM-11	110	tridimensional interconnecting 10-ring pores, $0.51 \text{ nm} \times 0.55 \text{ nm}$
ferrierite	110	pseudo-spherical cages with $\varnothing \approx 0.7$ nm, two 8-ring openings, $0.35 \times 0.48$ nm
	165	bidimensional interconnecting 10-ring pores, $0.42 \text{ nm} \times 0.55 \text{ nm}$
ZSM-5	113	tridimensional interconnecting 10-ring pores, 0.51 mm $\times$ 0.55 nm and 0.53 nm $\times$ 0.56 nm
rho	114	tridimensional interconnecting pores forming spherical cages with $\emptyset \approx 1.0$ nm,
	230	prisms, 8-ring, 0.36 nm
mordenite	115	unidimensional 12-ring pores, 0.65 nm $\times$ 0.70 nm,
	250	8-ring side-pockets, 0.26 nm × 0.57 nm

Table 1

<sup>129</sup>Xe NMR spectroscopy is a suitable method for **investigating the crystallinity and the presence of intergrowths of zeolites** [1]. The <sup>129</sup>Xe NMR intensity is not only proportional to the quantity of <sup>129</sup>Xe atoms adsorbed per cage, but also to the number of cages. Consequently, if a sample consists of a mixture of zeolites with different structure types or exchanged with cations of different sizes, the <sup>129</sup>Xe NMR spectrum is a direct measure of the composition of the sample. Furthermore, <sup>129</sup>Xe NMR spectroscopy can be applied to **investigate the blockage of certain pores**, e.g. by formation of coke in zeolite particles [10-12].

To fill up zeolite pores and cages for determining the free volume by measuring the number of particular <sup>129</sup>Xe atoms in these pores and cages, low-temperature <sup>129</sup>Xe NMR studies of <sup>129</sup>Xe atoms in zeolites with high coverage, [Xe], are useful [13]. Furthermore, <sup>129</sup>Xe atoms condensed inside the zeolite cages have a resonance signal significantly different from that of <sup>129</sup>Xe atoms condensed on the exterior surface of the zeolite micro-crystallite, which becomes visible, if the rapid exchange is frozen by low temperature. This method is utilized, e.g. for the investigation of dealuminated zeolites with a variety of mesopores and secondary cavities [14, 15]. For enhancing the sensitivity, in numerous **low- and variable-temperature** <sup>129</sup>Xe **NMR** studies, hyperpolarized (HP) xenon gas was utilized (see next page) [16-19, 26-31].

As an example, **Fig. 2** shows **variable-temperature HP** <sup>129</sup>**Xe NMR** spectra of **partially mesoporous ZSM-5** (MZSM-5-A in Ref. [17]). In these spectra, a series of signals at  $\delta_{129Xe} = 0$  ppm occur, which are due to <sup>129</sup>Xe atoms in the gas phase. The signals (a) at  $\delta_{129Xe} = 114$  to 176 ppm correspond to those of conventional zeolites ZSM-5 in the temperature range of = 293 to 153 K ( $\delta_{129Xe} = 113$  ppm for room temperature in **Table 1** [1]), ascribed to <sup>129</sup>Xe atoms in 10-ring pores. The above-

variable-temperature HP <sup>129</sup>Xe NMR spectra of partially mesoporous ZSM-5

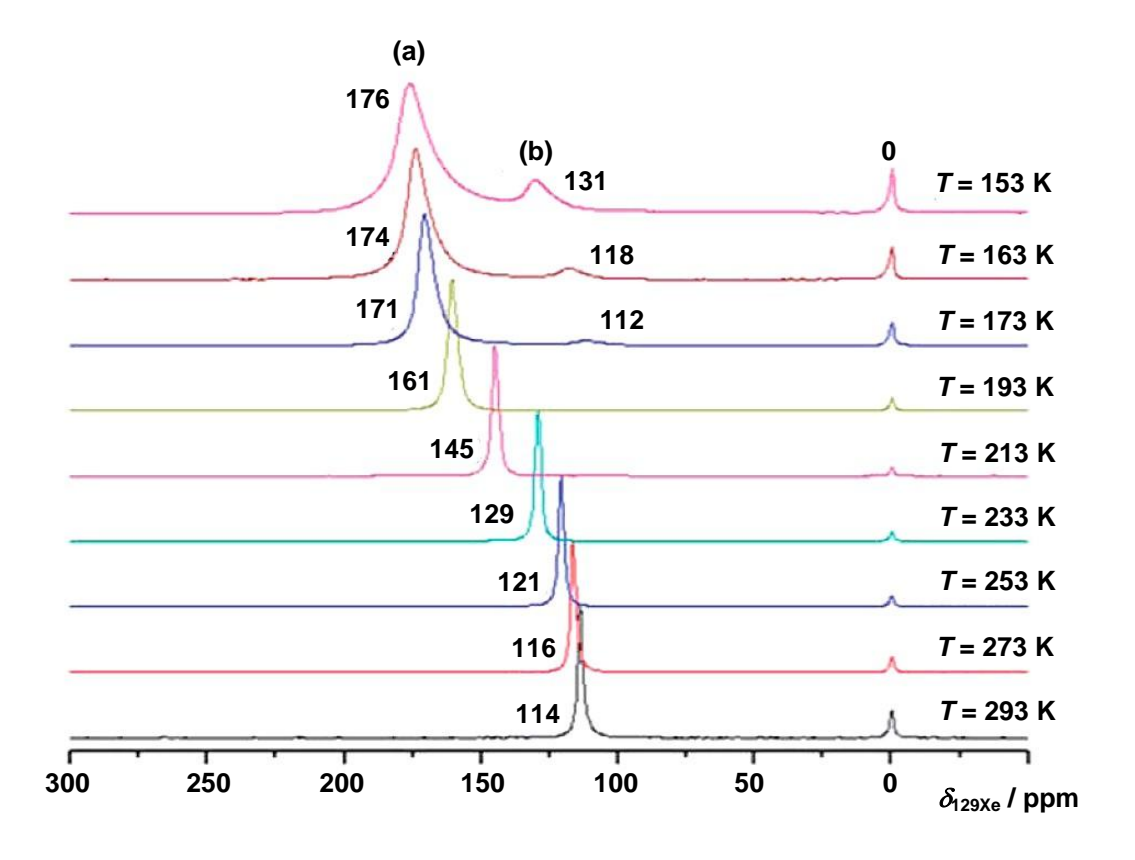
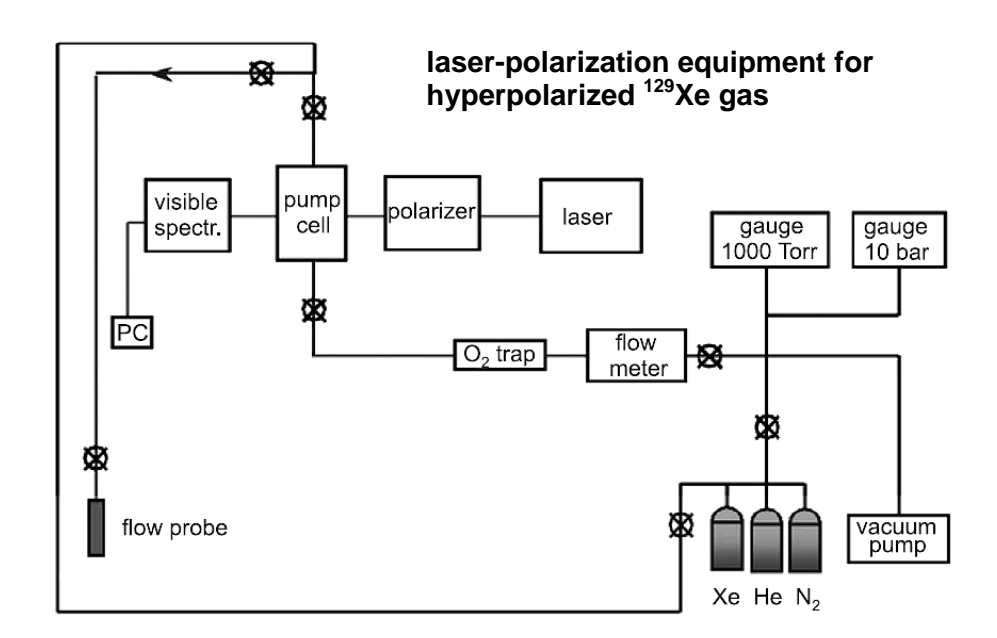


Fig. 2

mentioned resonance shift is a normal trend for the signals of  $^{129}$ Xe atoms in porous materials in variable-temperature experiments, mainly resulting from the increasing interaction of these atoms with the zeolite walls and the Xe-Xe interactions at lower temperatures. In the low temperature range from T = 173 to 153 K, an additional upfield series of signals (b) appears at  $\delta_{129Xe} = 112$  to 131 ppm, which hints at the mesoporosity of zeolite MZSM-5-A. Hence, the low temperature spectra clearly evidence that more than one type of pore environments exists in zeolite MZSM-5-A. Furthermore, the ratio of their free volumes corresponds to the ratio of the intensities of the  $^{129}$ Xe NMR signals (a) and (b) at low temperature in Fig. 2, top [17].

The *in situ* flow MAS NMR technique described in Refs. [20] and [21] (see also Section "flow probe 1", accessible via link "*In Situ* Solid-State NMR Techniques") allows the application of <sup>129</sup>Xe atoms with hyperpolarized (HP) nuclear spins. Optical pumping of <sup>129</sup>Xe nuclei leads to a strong increase of the sensitivity by 4 to 6 orders of magnitude higher than the thermal polarization. In **Fig. 3**, a schematic diagram of the optical pumping device is shown [22]. Circularly polarized light from a 60 W diode array laser is used for optical pumping at the D<sub>1</sub> transition of rubidium ( $\lambda$  = 794.7 nm) within a Pyrex pumping cell containing a small amount of rubidium vapor. The gas mixture containing 1% natural abundance xenon and 99% He, purified using an oxygen trap, is admitted into the optical pumping cell at a pressure of 2 bar in the fringe field of the superconducting magnet. Spin exchange during gasphase collisions between rubidium and xenon atoms results in a <sup>129</sup>Xe non-



equilibrium **nuclear spin polarization of ca. 5 to 8%**. After spin exchange with rubidium and being passed through the pumping cell, a plastic needle valve is used to expand the xenon gas to atmospheric pressure and to control the gas flow into the *in situ* flow MAS NMR probe. In Ref. [22], the advantage of hyperpolarized <sup>129</sup>Xe was demonstrated for studies of porous solids, such as of zeolites AIPO<sub>4</sub>-41, Ferrierite, and ITQ-6. See Ref. [33] for a review on the application of hyperpolarized <sup>129</sup>Xe NMR in catalysis.

As an example, **Fig. 4** shows **HP** <sup>129</sup>**Xe solid-state NMR spectra of zeolite ITQ-6**, which is a delaminated zeolite Ferrierite, recorded under a flow of hyperpolarized <sup>129</sup>Xe atoms without sample spinning (bottom) and with sample spinning rates of  $\nu_{\text{rot}}$  = 1 to 3 kHz (top) [22]. The signal at  $\delta_{129\text{Xe}}$  = 65 ppm, which is not observed for highly crystalline zeolite Ferrierite, is caused by xenon in the inter-lamellar space of zeolite ITQ-6. The two signals at  $\delta_{129\text{Xe}}$  = 100 and 135 ppm correspond to <sup>129</sup>Xe adsorbed in small cages and in channels, respectively. The comparison of the spectra recorded without and with MAS techniques demonstrates the advantage of sample spinning for reaching a good spectral resolution.

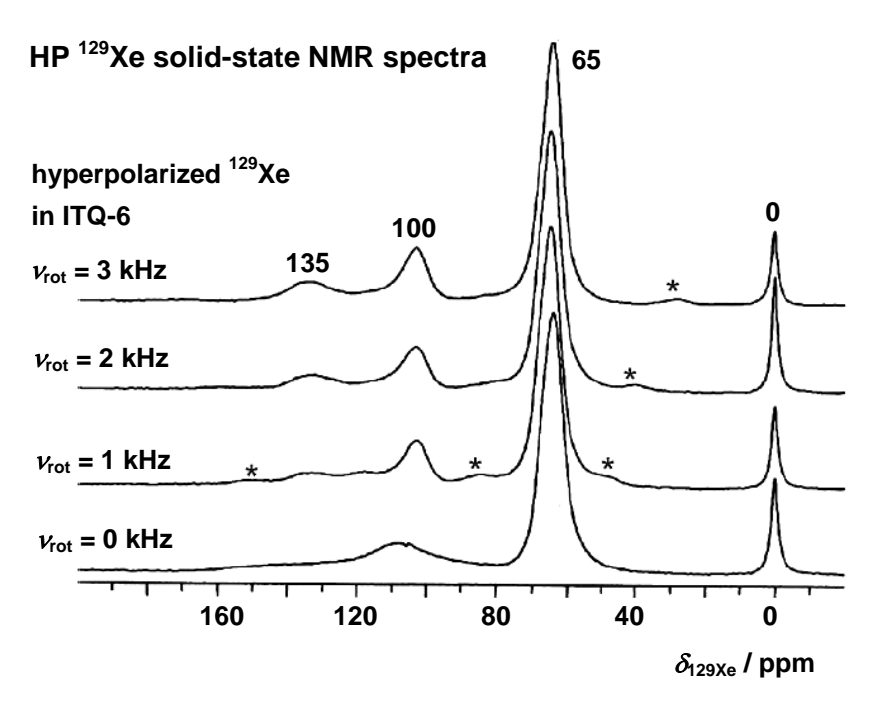


Fig. 4

The application of the laser-polarization equipment depicted in **Fig. 3** combined with an *in situ* flow MAS NMR probe allows 2D-exchange HP <sup>129</sup>Xe MAS NMR

experiments within a reasonable measurement time. Generally, 2D-exchange NMR experiments monitor changes in resonance frequencies occurring on a time scale ranging from milliseconds to few seconds. This is reached by monitoring the resonance frequencies before and after the mixing time,  $\tau_m$ , during which spin exchange occurs. These frequency changes are manifested by off-diagonal peaks in the 2D-exchange NMR spectrum, which depend on the duration of the mixing time [23].

The 2D-exchange HP <sup>129</sup>Xe MAS NMR spectrum of ITQ-6 in Fig. 5 was obtained with a mixing time of  $\tau_{\rm m}=50$  ms and consists of diagonal peaks at  $\delta_{\rm 129Xe}=65$ , 110, and 135 ppm with the cross peaks (a) to (c) [22]. These cross peaks indicate a <sup>129</sup>Xe exchange between the gas phase and the inter-lamellar space (a), between small cages and the inter-lamellar space (b), and between <sup>129</sup>Xe atoms in the channels and small cages (c). The diagonal peak for <sup>129</sup>Xe adsorbed in the channels ( $\delta_{\rm 129Xe}=135$  ppm) has a strongly elongated shape along the diagonal, while the diagonal peak of <sup>129</sup>Xe in the small cages ( $\delta_{\rm 129Xe}=100$  ppm) has an asymmetric shape. The elongated shape results from a distribution of slightly different adsorption sites in the channels.



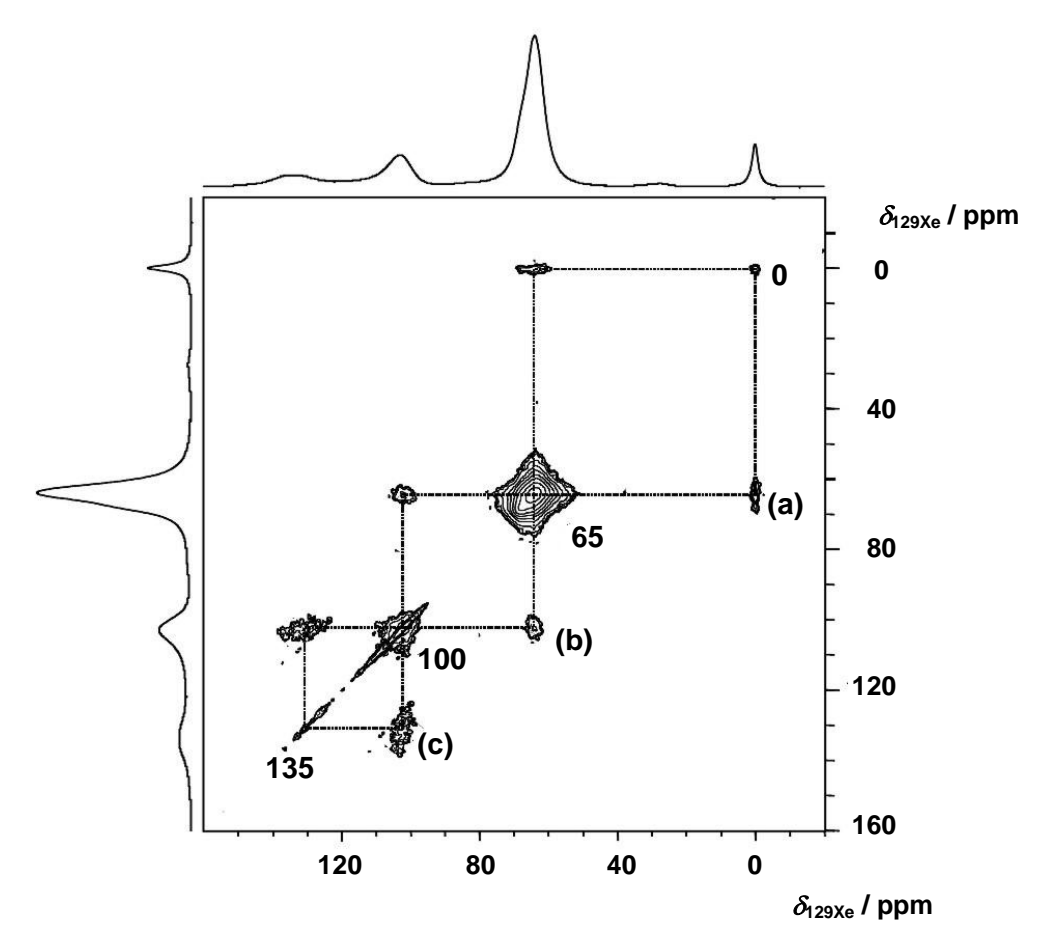


## Fig. 5

Similar like the study of pore blockage by formation of coke in zeolite particles [10-12], <sup>129</sup>Xe NMR spectroscopy was applied for investigating the presence and location of adsorbate molecules and reactants in zeolite particles [1, 24, 25, 32]. As an example, Fig. 6 shows a series of in situ HP 129Xe MAS NMR spectra, recorded during the adsorption of methanol on a zeolite CHA at T = 298 K for 30 min [24]. Theses spectra were obtained by utilizing an in situ flow MAS NMR probe equipped with an injection system similar to that described in Refs. [20] and [21]. The signals at  $\delta_{129Xe}$  = 0 ppm are due to <sup>129</sup>Xe atoms in the gas phase. All signals at lower field are originated from <sup>129</sup>Xe atoms adsorbed in CHA nanocages. Before introduction of methanol, the chemical shift of <sup>129</sup>Xe atoms in empty cages is  $\delta_{129Xe}$  = 84 ppm. After methanol is co-injected with the HP <sup>129</sup>Xe atoms into the MAS rotor, another signal appears at  $\delta_{129Xe} \cong 99$  ppm, which is due to  $^{129}Xe$  atoms co-adsorbed with methanol in the CHA cages. With increasing the adsorption time, its intensity increases, whereas the signal of <sup>129</sup>Xe atoms in empty cages decreases. Finally, after about 15 min, there is only one signal at  $\delta_{129Xe} \cong 99$  ppm, indicating that the adsorption of methanol reached the steady state [24].

# in situ HP <sup>129</sup>Xe MAS NMR spectroscopy of methanol adsorption on zeolite CHA

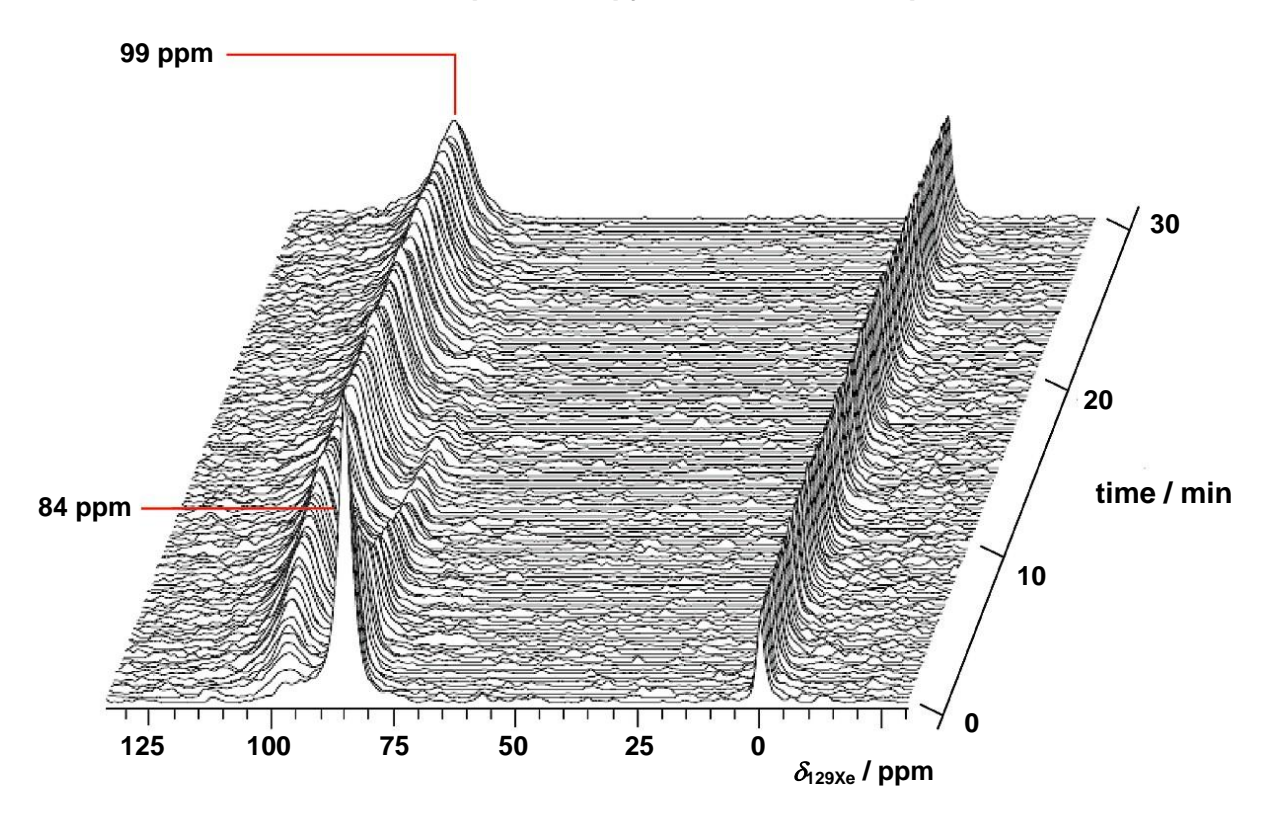


Fig. 6

**Catalyst preparation:** For the <sup>129</sup>Xe NMR studies leading to the shift values in **Fig. 1** and **Table 1** [1], zeolite powder was placed in an NMR tube and evacuated under vacuum at  $10^{-5}$  Torr at T = 298 K, and then at a temperature raised slowly to values between T = 573 and 873 K and maintained at this value for 8 h. The adsorption of xenon gas (99.99 %) was performed on a classical volumetric apparatus [1, 6].

Before the measurements leading to the spectra in **Fig. 2** [17], the samples were dehydrated at T = 673 K under vacuum (<  $10^{-5}$  Torr) for 24 h.

For the studies leading to **Figs. 4 and 5** [22], the sample materials were activated at T = 473 K in high vacuum, then packed into the rotor using a glove box under argon atmosphere. The filled rotor was then inserted into the probe and purged with the gas mixture during the entire duration of the experiment. Before recording the NMR spectra, and in order to remove water or oxygen possibly adsorbed during the insertion of the rotor into the probe, the sample was heated to T = 373 K. After this procedure the sample is cooled to the desired measurement temperature [22].

Prior to the *in situ* MAS NMR experiments leading to **Fig. 6** [24], about 100 mg samples were dehydrated at T = 673 K for 20 h in vacuum (<  $10^{-2}$  Pa).

<sup>129</sup>Xe NMR studies: The <sup>129</sup>Xe NMR spectra leading to the shift values summarized in **Table 1** were recorded at ambient temperature using a 90 MHz Bruker Fourier-transform pulse spectrometer operating at the <sup>129</sup>Xe resonance frequency of  $\nu_0$  = 24.9 MHz.

The variable-temperature HP  $^{129}$ Xe NMR spectra in **Fig. 2** were recorded on a Varian Infinity-plus 400 spectrometer at the  $^{129}$ Xe resonance frequency of  $\nu_0$  = 110.6 MHz, using a 7.5 mm probe, with a  $\pi$ /2 pulse width of 3  $\mu$ s, 100 to 200 scans, and a recycle delay of 2 s [17].

The spectra in **Figs. 4 and 5** were acquired on a Bruker AMX300 spectrometer operating at the  $^{129}$ Xe resonance frequency of  $\nu_0$  = 83.02 MHz [22]. For the HP  $^{129}$ Xe injection, a conventional Bruker 7 mm MAS probe with MASCAT stator with a sample spinning up to  $\nu_{\text{rot}}$  = 3.5 kHz was utilized. The basic principles of the 2D-exchange NMR experiment are described in Ref. [23].

The spectra in **Fig. 6** were recorded on Varian Infinityplus-400 spectrometer at the  $^{129}$ Xe resonance frequency of  $v_0 = 110.6$  MHz with a  $\pi/2$  pulse width of 3  $\mu$ s, a 1s recycle delay and 10 scans. The samples were spun at  $v_{\text{rot}} = 3$  kHz under continuous

flow using a 7.5 mm rotor [24]. A continuous flow of a gas mixture, consisting of 1% Xe, 1%  $N_2$ , and 98% He, was injected into the *in situ* flow MAS NMR probe at the rate of 100 mL/min with or without methanol, bubbled with dry nitrogen at the rate of 10 mL/min [24].

In the above-mentioned studies, flow MAS NMR probes constructed according to the principle described in Refs. [20] and [21] were used.

Equipment for producing hyperpolarized <sup>129</sup>Xe gas is described in Refs. [22], [24], and [33].

For all <sup>129</sup>Xe NMR studies, the reference signal was that of xenon gas extrapolated to a pressure of zero ( $\delta_{129Xe} = 0$  ppm).

#### References:

- [1] J. Fraissard, T. Ito, <sup>129</sup>Xe n.m.r. study of adsorbed xenon: A new method for studying zeolites and metal-zeolites, Zeolites 8 (1988) 350-361, DOI: 10.1016/S0144-2449(88)80171-4.
- [2] P.J. Barrie, J. Klinowski, <sup>129</sup>Xe NMR as a probe for the study of microporous solids A critical review, Progr. Nucl. Magn. Reson. Spectrosc. 24 (1992) 91-108, DOI: 10.1016/0079-6565(92)80006-2.
- [3] J. Demarquay, J. Fraissard, <sup>129</sup>Xe NMR of xenon adsorbed on zeolites. Relationship between the chemical shift and the void space, Chem. Phys. Lett. 136 (1987) 314-318, DOI: <u>10.1016/0009-2614(87)80258-0</u>.
- [4] D.W. Johnson, L. Griffiths, *Application of xenon-129 n.m.r. to the characterization of zeolites*, Zeolites 7 (1987) 484-487, DOI: 10.1016/0144-2449(87)90021-2.
- [5] E.G. Derouane, J.B. Nagy, Surface curvature effects on the NMR chemical shift for molecules trapped in microporous solids, Chem. Phys. Lett. 137 (1987) 341-344, DOI: 10.1016/0009-2614(87)80896-5.
- [6] T. Ito, J. Fraissard, <sup>129</sup>Xe NMR study of xenon adsorbed on Y zeolites, J. Chem. Phys. 76 (1982) 5225-5229, DOI: <u>10.1063/1.442917</u>.
- [7] M.E. Davis, C. Saldarriaga, C. Montes, B.E. Hanson, Characterization of aluminum phosphate and SAPO molecular sieves by xenon-129 NMR spectroscopy, J. Phys. Chem. 92 (1988) 2557-2560, DOI; 10.1021/j100320a032.
- [8] Q.J. Chen, J. Fraissard, H. Cauffriez, J.L. Guth, <sup>129</sup>Xe n.m.r. study of VPI-5 and AIPO<sub>4</sub>-8 molecular sieves, Zeolites 11 (1991) 534-538, DOI: 10.1016/S0144-2449(05)80001-6.

- [9] M.J. Annen, M.E. Davis, B.E. Hanson, <sup>129</sup>Xe NMR spectroscopy on molecular sieves SAPO-37, AIPO<sub>4</sub>-5, SAPO-5 and SSZ-24, Catal. Lett. 6 (1990) 331-340, DOI: 10.1007/BF00763999.
- [10] M.C. Barrage, J.L. Bonardet, J. Fraissard, <sup>129</sup>Xe-NMR study of coke distribution in dealuminated HY zeolites, Catal. Lett. 5 (1990) 143-154, DOI: 10.1007/BF00763946.
- [11] J.L. Bonardet, M.C. Barrage, J. Fraissard, *Use of NMR techniques for studying deactivation of zeolites by coking*, J. Mol. Catal. A: Chemical 96(2) (1995) 123-143, DOI: 10.1016/1381-1169(94)00030-1.
- [12] J.-L. Bonardet, T. Domeniconi, P. N'Gokoli-Kékélé, M.-A. Springuel-Huet, J. Fraissard, *Hydrocarbon diffusion measurements and coke distribution in zeolite pellets: A study by* <sup>1</sup>*H NMR imaging and* <sup>129</sup>*Xe NMR spectroscopy*, Langmuir 15 (1999) 5836-5840, DOI: 10.1021/la981308v.
- [13] T.T.P. Cheung, C.M. Fu, S. Wharry, <sup>129</sup>Xe NMR of xenon adsorbed in Y zeolites at 144 K, J. Phys. Chem. 92 (1988) 5170-5180, DOI: 10.1021/j100329a022.
- [14] T.T.P. Cheung, C.M. Fu, Low-temperature (144 K) <sup>129</sup>Xe NMR studies of steam-dealuminated Y zeolites, J. Phys. Chem. 93 (1989) 3740-3747, DOI: 10.1021/j100346a073.
- [15] M. Gackowski, A. Selent, I. Ainasoja, M. Mazur, M. Hunger, J. Datka, V.-V. Telkki, Cleansing effect during the TBAOH treatment of ultra-stable zeolite Y, Microporous Mesoporous Mater. 359 (2023) 112626, DOI: 10.1016/j.micromeso.2023.112626.
- [16] L.-H. Chen, S.-T. Xu, X.-Y. Li, G. Tian, Y. Li, J.C. Rooke, G.-S. Zhu, S.-L. Qiu, Y.-X. Wei, X.-Y. Yang, Z.-M. Liu, B.-L. Su, *Multimodal Zr-Silicalite-1 zeolite nanocrystal aggregates with interconnected hierarchically micro-meso-macroporous architecture and enhanced mass transport property*, J. Colloid. Interf. Sci. 377 (2012) 368-374, DOI: 10.1016/j.jcis.2012.03.018.
- [17] Q. Wang, S. Xu, J. Chen, Y. Wei, J. Li, D. Fan, Z.i Yu, Yue Qi, Y. He, S. Xu, C. Yuan, Y. Zhou, J. Wang, M. Zhang, B. Su, Z. Liu, Synthesis of mesoporous ZSM-5 catalysts using different mesogenous templates and their application in methanol conversion for enhanced catalyst lifespan, RSC Adv. 4 (2014) 21479-21491, DOI: 10.1039/c4ra02695k.
- [18] J. Hollenbach, C. Kuester, H. Uhlig, M. Wagner, B. Abel, Roger Glaeser, W.-D. Einicke, D. Enke, J. Matysik, *Hyperpolarized* <sup>129</sup>Xe NMR as an alternative approach for investigating structure and transport in ordered mesoporous materials prepared via pseudomorphic transformation, J. Phys. Chem. C 121 (2017) 15804-15814, DOI: 10.1021/acs.jpcc.7b04365.

- [19] Z. Zhao, X. Li, S. Li, S. Xu, X. Bao, Y. Bilge, P. Andrei-Nicola, U. Mueller, W. Zhang, *Structural investigation of interlayer-expanded zeolite by hyperpolarized* <sup>129</sup>Xe and <sup>1</sup>H NMR spectroscopy, Microporous Microporous Mater. 288 (2019) 109555, DOI: 10.1016/j.micromeso.2019.06.017.
- [20] M. Hunger, T. Horvath, A new MAS NMR probe for in situ investigations of hydrocarbon conversion on solid catalysts under continuous-flow conditions, J. Chem. Soc., Chem. Commun. (1995) 1423-1424, DOI: 10.1039/c39950001423.
- [21] M. Hunger, In situ flow MAS NMR spectroscopy: State of the art and applications in heterogeneous catalysis, Prog. Nucl. Magn. Reson. Spectrosc. 53 (2008) 105-127, DOI: 10.1016/j.pnmrs.2007.08.001
- [22] A. Nossov, F. Guenneau, M.-A. Springuel-Huet, E. Haddad, V. Montouillout, B. Knott, F. Engelke, C. Fernandez, A. Gedeon, *Continuous flow hyperpolarized*129 Xe-MAS NMR studies of microporous materials, Phys. Chem. Chem. Phys. 5 (2003) 4479-4483, DOI: 10.1039/B305793N.
- [23] J. Jeener, B.H. Meier, P. Bachmann, R.R. Ernst, *Investigation of exchange processes by two-dimensional NMR spectroscopy*, J. Chem. Phys. 71 (1979) 4546-4553, DOI: 10.1063/1.438208.
- [24] S. Xu, W. Zhang, X. Liu, X Han, X. Bao, *Enhanced in situ continuous-flow MAS NMR for reaction kinetics in the nanocages*, J. Am. Chem. Soc. 131 (2009) 13722-13727, DOI: 10.1021/ja904304h.
- [25] S. Gao, S. Xu, Y. Wei, Q. Qiao, Z. Xu, X. Wu, M. Zhang, Y. He, S. Xu, Z. Liu, Insight into the deactivation mode of methanol-to-olefins conversion over SAPO-34: Coke, diffusion, and acidic site accessibility, J. Catal. 367 (2018) 306-314, DOI: 10.1016/j.jcat.2018.09.010.
- [26] X.J. Li, W.P. Zhang, S.L. Liu, L. Xu, X. Han, X. Bao *The role of alumina in the supported Mo/Hbeta-Al*<sub>2</sub>O<sub>3</sub> catalyst for olefin metathesis: a high-resolution solid-state NMR and electron microscopy study, J. Catal. 250 (1) (2007) 55-66, DOI: 10.1016/j.jcat.2007.05.019.
- [27] M.A. Springuel-Huet, A. Nossov, Z. Adem, F. Guenneau, C. Volkringer, T. Loiseau, G. Ferey, A. Gedeon, <sup>129</sup>Xe NMR study of the framework flexibility of the porous hybrid MIL-53(AI), J. Am. Chem. Soc. 132 (33) (2010) 11599-11607, DOI: 10.1021/ja103105y.
- [28] C.D. Keenan, M.M. Herling, R. Siegel, N. Petzold, C.R. Bowers, E.A. Rooessler, J. Breu, J. Senker, *Porosity of pillared clays studied by hyperpolarized* <sup>129</sup>Xe NMR spectroscopy and Xe adsorption isotherms, Langmuir 29 (2013) 643-652, DOI: 10.1021/la304502r.
- [29] F. Guenneau, K. Panesar, A. Nossov, M.A. Springuel-Huet, T. Azais, F. Babonneau, C. Tourne-Peteilh, J.-M. Devoisselle, A. Gedon, *Probing the*

- mobility of ibuprofen confined in MCM-41 materials using MAS-PFG NMR and hyperpolarised-<sup>129</sup>Xe NMR spectroscopy, Phys. Chem. Chem. Phys. 15 (2013) 18805-18808, DOI: 10.1039/c3cp52695j.
- [30] M.A. Springuel-Huet, A. Nossov, F. Guenneau, A. Gedeon, Flexibility of ZIF-8 materials studied using <sup>129</sup>Xe NMR, Chem. Commun. 49 (67) (2013) 7403-7405, DOI: 10.1039/c3cc43119c.
- [31] T.W. Kemnitzer, C.B.L. Tschense, T. Wittmann, E.A. Roessler, J. Senker, Exploring local disorder within CAU-1 frameworks using hyperpolarized <sup>129</sup>Xe NMR spectroscopy, Langmuir 34 (42) (2018) 12538-12548, DOI: 10.1021/acs.langmuir.8b02592.
- [32] S. Xu, X. Li, C. Sun, A. Zheng, X. Han, X. Liu, X. Bao, *Mapping the dynamics of methanol and xenon co-adsorption in SWNTs by in situ continuous-flow hyperpolarized* <sup>129</sup>Xe NMR, Phys. Chem. Chem. Phys. 21 (6) (2019) 3287-3293, DOI: 10.1039/c8cp07238h.
- [33] B. Fan, S. Xu, Y. Wei, Z. Liu, *Progresses of hyperpolarized* <sup>129</sup>Xe NMR application in porous materials and catalysis, Magn. Reson. Lett. 1 (2021) 11-27, DOI: 10.1016/j.mrl.2021.100005.